ROYAL SOCIETY
OF CHEMISTRY

HIGHLIGHT

Check for updates

Rapid advances in antimony triselenide photocathodes for solar hydrogen generation

Wooseok Yang (ID) and Jooho Moon (ID) *

One of the paramount challenges for realizing practical solar hydrogen production is the development of a low-cost semiconductor that is suitable for large-area and high-performance photoelectrochemical devices. Antimony triselenide (Sb_2Se_3) has emerged as a nearly ideal semiconductor material that satisfies nearly all requirements for effectively generating hydrogen using solar energy. In this report, we highlight the extraordinary characteristics of Sb_2Se_3 relative to the myriad of other emerging semiconductors, in terms of cost, band gap, optoelectronic properties, photocorrosion stability, and processability. Additionally, we discuss recent studies on Sb_2Se_3 photocathodes with a focus on their intrinsic properties, use of co-catalysts, and top and bottom interface engineering for enhanced performance. Unresolved issues and future research directions will also be discussed briefly. We believe that the rapid advances in Sb_2Se_3-photocathode water splitting over the past three years suggest a positive outlook for the cost-effective production of solar hydrogen.

1. Introduction

Extreme weather events caused by global climate change are becoming increasingly frequent, and the world is recognizing the urgent need to implement carbon-neutral energy systems for a sustainable society. Solar hydrogen production through the splitting of water is an attractive technique for obtaining hydrogen as a carbon-free energy carrier by leveraging renewable solar energy. Since the first demonstration of photoelectrochemical (PEC) water splitting in the 1970s,[1] significant advancements in generating hydrogen using solar energy have been achieved. However, despite extensive research, solar-to-fuel systems are still at the level of basic technology research, which is far from commercialization.[2,3] Considering the target solar-to-hydrogen (STH) efficiency (η_{STH} above 10%)[4] and the efficiency achieved by a III–V semiconductor-based dual-junction tandem cell (η_{STH} approximately 19%),[5] it is clear that efficiency is not the major bottleneck for the commercialization of PEC water splitting. Commercialized photovoltaic technologies are overwhelmingly dominated by Si solar cells despite the greater efficiencies of alternative technologies,[6] indicating that lower efficiency levels obtained using cost-effective systems are preferable to highly efficient yet expensive systems. Likewise, in PEC water splitting systems, cost must be reduced while maintaining reasonable efficiency, to realize solar hydrogen production at a commercial scale.

The most important building blocks in PEC water splitting systems in terms of cost and performance are light-absorbing semiconductors. In the high STH systems based on III–V semiconductors, the cost of semiconductor materials is relatively large compared to that of other parts. For example, the cost of InGaP/GaAs ($175) per unit solar collection area is much greater than that of other parts, such as catalysts (Pt and IrO_x, $8) and membranes (127 μm-thick Nafion, $5).[7] Therefore, the development of cost-effective light absorbers with desirable properties is a key challenge that must be overcome to facilitate economically viable PEC water splitting.[8]

The typical requirements for semiconductors for PEC water splitting are presented in Fig. 1. In this paper, we aim to demonstrate how antimony triselenide (Sb_2Se_3) satisfies nearly all of these requirements. Regarding the details of other candidate materials, interested readers can refer to previous comprehensive reviews on semiconductor materials.[9,10] The first screening criterion is the cost of semiconductor materials, which expensive III–V semiconductors are unable to satisfy. Among cost-effective semiconductors, large-band-gap (E_g) semiconductors, such as TiO_2 ($E_g \approx 3.2$ eV) and WO_3 ($E_g \approx 2.8$ eV), are unsuitable for harvesting a broad range of photons based on their large E_g values. Hematite (α-Fe_2O_3) is another low-cost semiconductor with a relatively small E_g value (approximately 2.1 eV). However, an extremely short minority carrier diffusion length (2–4 nm) and low electron mobility (approximately 10^{-2} cm^2 V^{-1} s^{-1}) limit its performance severely.[11] Photocorrosion stability is another particularly important issue in PEC water splitting. Although earth-abundant Cu_2O has favorable characteristics, including a relatively small band gap ($E_g \approx 2.0$ eV), reasonable carrier diffusion length (up to 200 nm),[12] and desirable hole mobility (approximately 5 cm^2 V^{-1} s^{-1}),[13] it experiences significant

Department of Materials Science and Engineering, Yonsei University, 50 Yonsei-ro, Seodaemun-gu, Seoul, 03722, Republic of Korea. E-mail: jmoon@yonsei.ac.kr
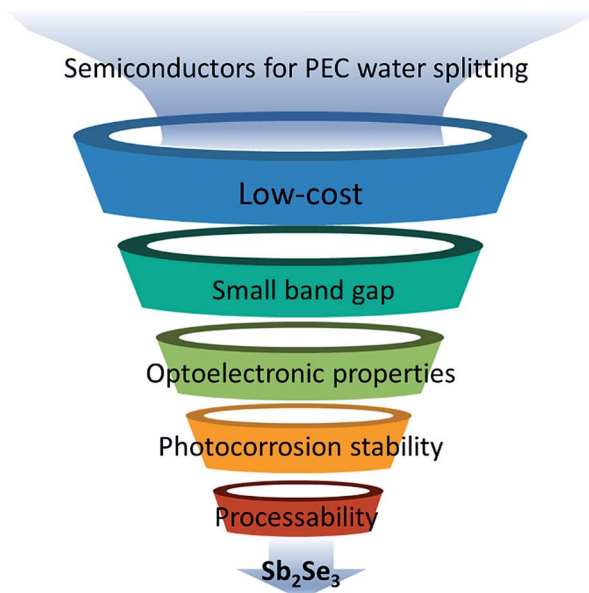
This journal is © The Royal Society of Chemistry 2019

J. Mater. Chem. A, 2019, 7, 20467–20477 | 20467

Fig. 1 The requirements for an ideal semiconductor for PEC water splitting, highlighting the uniqueness of Sb_2Se_3 as a nearly ideal semiconductor.

photocorrosion because the redox potentials for oxidation and reduction potential of Cu_2O lie within its band gap, resulting in rapid degradation of photocurrent.[14] The final criterion is processability, meaning phase-pure semiconducting material can be readily synthesized in a cost-effective manner. Numerous materials suffer from significant difficulty in obtaining pure crystals based on detrimental secondary phases and harsh processing conditions. For example, $CuFeO_2$ ($E_g \approx 1.5$ eV) is a low-cost and photocorrosion resistant semiconductor with good carrier diffusion length (approximately 225 nm).[15,16] However, $CuFeO_2$ generally requires a high-temperature annealing process at approximately 700 °C, which can lead to the formation of secondary phases, such as CuO and Fe_2O_3.[17] It should be noted that a lack of phase purity can result in more significant problems in large-scale devices, such as inhomogeneity in the spatial distribution of potentials based on secondary phases spread over a large area.[18] In addition to the metal oxides, there are some cost-effective metal selenide semiconductors exhibiting good optoelectronic properties. Nathan Lewis and co-workers reported p-type single-crystalline WSe_2 photocathodes by a chemical vapor transport method, revealing high photocurrent density ($\sim$25 mA cm^{-2} at 0 V *versus* a reversible hydrogen electrode (V_{RHE})).[19] Polycrystalline WSe_2 photocathodes were fabricated by a magnetron sputtering-based method,[20–22] but the performance ($\sim$5.6 mA cm^{-2} at 0 V_{RHE}) was relatively lower than that of the single-crystalline one. As a more scalable processing for WSe_2 photocathodes, solution processing of exfoliated WSe_2 nanoflakes was developed by Sivula and co-workers.[23,24] However, the solution-processed WSe_2 photocathodes revealed much lower photocurrent density ($\sim$4 mA cm^{-2} at 0 V_{RHE}). Therefore, a low-cost semiconductor suitable for a cost-effective fabrication method

should be developed for practical STH conversion. In the following sections, we highlight the uniqueness of Sb_2Se_3 as a nearly ideal semiconductor for PEC water splitting by surveying recent research on Sb_2Se_3 photocathodes.

2. Recent studies on Sb_2Se_3 photocathodes

The crystal structure of Sb_2Se_3 was reported more than 50 years ago.[25] Early studies on this material were mostly related to its phase formation, reflectivity, and desirable thermoelectric and semiconducting properties compared to other chalcogenide materials.[26–28] The first two notable photovoltaic devices, namely Sb_2Se_3 thin films and Sb_2Se_3-sensitized solar cells, were reported at the nearly same time in 2014.[29,30] Since then, the power conversion efficiency of Sb_2Se_3 thin film solar cells has rapidly increased from an initial value of 2.26% to the maximum recorded value of 9.2%.[31] In the field of PEC water splitting, the first Sb_2Se_3 photocathode was reported in early 2017.[32] Since then, extensive research on Sb_2Se_3 photocathodes has been pursued with a focus on the unique intrinsic properties of Sb_2Se_3, the use of earth-abundant co-catalysts, and top and bottom interface engineering, as shown in Fig. 2. It is worth noting that we focus on Sb_2Se_3 for PEC water splitting research, although photovoltaic research has also demonstrated the uniqueness of Sb_2Se_3 as a semiconductor.

2.1 Uniqueness of Sb_2Se_3 as a semiconductor for PEC water splitting

Sb_2Se_3 has several extraordinary features that make it a nearly ideal semiconductor for PEC water splitting. It satisfies nearly all of the aforementioned requirements. From the perspective of general light absorbers (*i.e.*, not only absorbers for PEC water splitting), Sb_2Se_3 is very cost effective. Fig. 3 shows the abundance and cost comparison for the elements of In, Ga, Mo, Sb and Cu. Although the abundance of Sb is relatively low (approximately 0.00002%) compared to Cu (0.0068%), the cost of Sb ($3.9 per lb) is similar to that of Cu ($3.0 per lb), which is much lower than the costs of other expensive elements used for light absorbers, such as In (approximately $172 per lb), Ga (approximately $160 per lb), and Mo (approximately $14 per lb).[33,34] Additionally, Sb_2Se_3 has high electron mobility (16.9 cm^2 V^{-1} s^{-1}) and diffusion length (1.7 $\pm$ 0.2 μm) along the *c* axis.[35] It
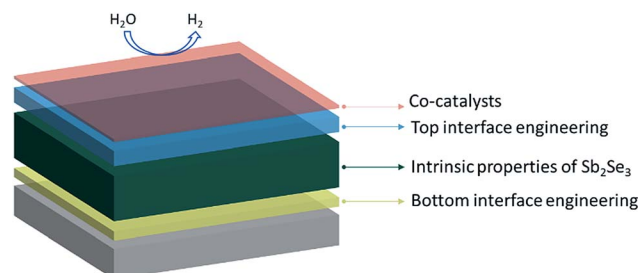
Fig. 2 Schematic summary of recent research trends related to Sb_2Se_3 photocathodes.

20468 | *J. Mater. Chem. A*, 2019, **7**, 20467–20477

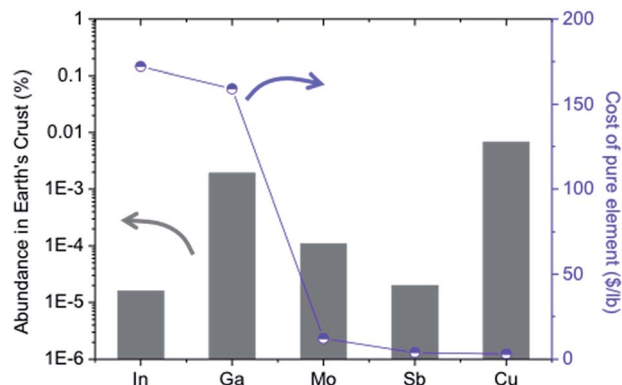This journal is © The Royal Society of Chemistry 2019

Fig. 3   Comparison of the abundance and the costs of elements used in light absorbers.

has also been reported that the transient terahertz mobility of Sb_2Se_3 can reach up to 600 cm^2 V^{-1} s^{-1} at a low fluence level,[36] which is much greater than the mobility of Cu_2O (approximately 8.5 cm^2 V^{-1} s^{-1}) under similar experimental conditions.[13] One intriguing aspect of Sb_2Se_3 that distinguishes it from other semiconductor materials is its excellent processability. Sb_2Se_3 has a low melting point of 608 °C compared to other light absorbers (e.g., $Cu_2O \sim$ 1232 °C) and a high saturated vapor pressure of approximately 1200 Pa at 550 °C, which enables low-temperature processing and various deposition techniques, including solution processing,[29] rapid thermal evaporation,[37] close-space sublimation,[31,38] and vapor transport deposition.[39] Therefore, it can be easily deposited on a flexible substrate to fabricate stable flexible solar cells with high power per unit weight,[40] as well as on a large area substrate over 20 cm^2 as demonstrated by Zhang et al.[41] Additionally, Sb_2Se_3 is a binary compound having a thermodynamically stable orthorhombic Pnma structure, which is centrosymmetric with 8 points of inversion per unit cell, with a fixed composition under ambient pressure.[42] It is noteworthy that although a different crystal

structure of a disordered bcc structure ($Im\bar{3}m$) can be formed under pressures over 50 GPa,[43] no severe secondary phase issues are expected during the practical fabrication of large-area Sb_2Se_3 thin films.

In addition to its attractive properties as a general light absorber, Sb_2Se_3 has additional features that are advantageous for PEC water splitting. Prabhakar et al.[44] demonstrated that Sb_2Se_3 thin films are robustly stable in terms of photocorrosion in a strong acid under 1-sun illumination conditions. Unlike other semiconducting materials, such as photocorrosive Cu_2O, no significant photocorrosion peaks can be observed in the cyclic voltammetry (CV) curves of a bare Sb_2Se_3 thin film, as shown in Fig. 4a. Even after 285 cycles of CV scans, a MoS_x catalyst-deposited Sb_2Se_3 photocathode exhibits similar performance compared to a freshly prepared MoS_x/Sb_2Se_3 photocathode, as shown in Fig. 4b, demonstrating the intrinsic stability of Sb_2Se_3.

The small E_g value of Sb_2Se_3 (approximately 1.2 eV) is another merit of Sb_2Se_3-based photocathodes for PEC water splitting. It should be noted that E_g larger than 1.9 eV is required to drive sufficient water splitting reactions due to the thermodynamically required potential (1.23 eV) and over-potentials for electrochemical reactions. However, there is a trade-off between photovoltage and light absorption, as the semiconductor having a larger E_g is capable of harvesting less amount of solar photons. Thus, a tandem cell configuration, consisting of two different types of semiconductors, is considered as the most efficient system to produce sufficient photovoltage and light absorption. Although a small-E_g semiconductor as a bottom photoelectrode is an indispensable element for achieving high η_{STH} values in a PEC tandem cell according to theoretical calculation,[45,46] there are limited candidate materials for high-performance PEC tandem devices. One promising material with a small E_g value is $Cu(In,Ga)Se_2$, whose E_g value varies from 1.0 eV to 1.5 eV depending on the In/Ga ratio.[47] However, despite its excellent performance,
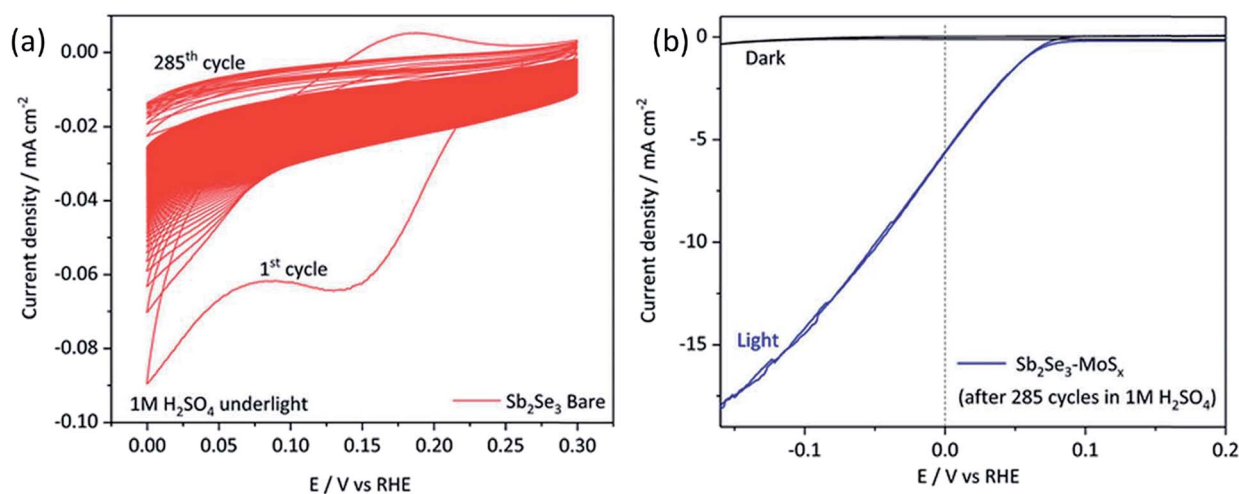

Fig. 4   (a) CV curves of a bare Sb_2Se_3 thin film in 1 M H_2SO_4 under 1-sun illumination. (b) Current density vs. potential plots of an $Sb_2Se_3–MoS_x$ photocathode prepared after 285 CV cycles of bare Sb_2Se_3, in 1 M H_2SO_4 under 1-sun illumination. Reproduced from ref. 44 with permission from The Royal Society of Chemistry.
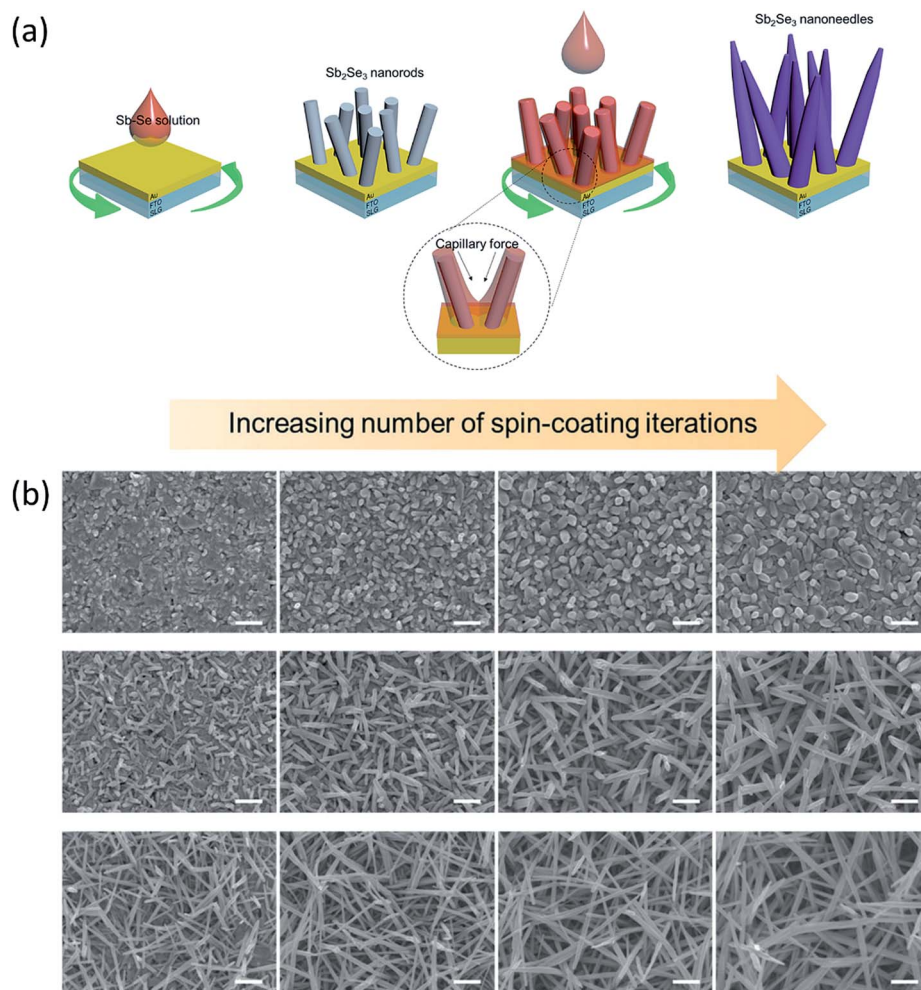
Fig. 5 (a) Schematic diagram showing the growth process of Sb_2Se_3 nanoneedles. Reproduced from ref. 32 with permission from The Royal Society of Chemistry. (b) Morphological evolution of Sb_2Se_3 nanostructures depending on the composition of solvents as a function of spin-coating iterations. The images in each column show Sb_2Se_3 film morphology after two, four, six, and eight coatings from the left (scale bar = 500 nm). Reproduced from ref. 50 with permission from John Wiley & Sons, Inc.

expensive In and Ga are unsuitable for the practical large-area applications. Si is another well-known small-E_g semiconductor (approximately 1.1 eV) for PEC water splitting. However, Si is an indirect-E_g semiconductor having a direct E_g value of 3.2 eV, resulting in weak absorption of visible-light photons. The weak absorption of Si means Si-based devices inevitably require a thick film to achieve sufficient light absorption, meaning high-purity single-crystalline Si wafers are required to minimize electrical loss. In contrast, the direct E_g value of Sb_2Se_3 is slightly greater than its indirect E_g value (0.01–0.1 eV),[48,49] resulting in the high absorption coefficient over 10^5 cm^{-1}. Therefore, an Sb_2Se_3 thin film with a thickness of 1 to 2 μm is able to absorb sufficient light. Furthermore, based on its novel one-dimensional (1D) crystal structure, the grain boundaries of Sb_2Se_3 are known to be electrically benign, meaning no significant recombination occurs at grain boundaries.[37] Given the aforementioned unique properties of Sb_2Se_3, we can reasonably postulate that Sb_2Se_3 is an unrivalled low-cost and small-E_g semiconductor for PEC water splitting.

2.2   Morphological control of Sb_2Se_3 photocathodes

Because one important uniqueness of Sb_2Se_3 is its strong anisotropic nature based on its 1D crystal structure, many studies on Sb_2Se_3 photocathodes have been associated with synthetic methods for generating varied morphologies of 1D Sb_2Se_3, resulting in structure-dependent performance. The first Sb_2Se_3 photocathode was fabricated with a 1D nanoneedle array morphology from a molecular solution obtained by mixing both Sb and Se solutions.[32] The Sb solution was prepared by dissolving $SbCl_3$ in 2-methoxyethanol, whereas Se powder was dissolved in a mixed solvent of thioglycolic acid (TGA) and ethanolamine (EA) to prepare the Se solution. The schematic in Fig. 5a shows that the Sb_2Se_3 nanoneedles were fabricated using a simple spin-coating method without a seed layer or vapor phase assistance. In a subsequent study, the authors demonstrated that the 1D structure of Sb_2Se_3 originates from the $[Sb_4Se_7]^{2-}$ chains present in molecular ink. Additionally, the aspect ratio of Sb_2Se_3 can be modified from 1D nanowires to nanorod arrays by simply modulating the solvent ratio between

TGA and EA (Fig. 5b).[50] By adjusting the aspect ratio of 1D Sb_2Se_3, the photocurrent density of the resulting Sb_2Se_3 photocathode was enhanced from its initial value of 2 mA cm^{-2} at 0 V *versus* a reversible hydrogen electrode (V_{RHE}) to 12.5 mA cm^{-2} at 0 V_{RHE}. The improved performance was attributed to newly facilitated charge carrier transport along well-oriented Sb_2Se_3 nanorod arrays with favorable orientations.

Another strategy for fabricating morphology-controlled Sb_2Se_3 photocathodes was developed using a stronger solvent, namely a combination of 2-mercaptoethanol and ethylenediamine, to facilitate the direct dissolution of metallic elements without the aid of chlorine anions.[51] The direct dissolution of metallic Sb is advantageous for minimizing the incorporation of unnecessary elements, such as oxygen and chlorine. Varying morphologies of Sb_2Se_3, ranging from particulate planar thin films to nanowires laid horizontally on the substrate, were obtained by modifying the relative ratio of Sb and Se in the ink solution, as shown in Fig. 6a–c. The formation mechanism of these 1D nanostructures is similar to that in the previous case using TGA and EA, where the excess selenium induced the formation of $[Sb_4Se_7]^{2-}$ chains, as confirmed by liquid Raman analysis. Additionally, a similar tendency in which the planar structure achieved superior performance (14 mA cm^{-2} at 0 V_{RHE}) compared to the elongated 1D nanostructure (10.5 mA cm^{-2} at 0 V_{RHE}) was observed in a different solvent system based on enhanced charge separation in a favorable direction, as illustrated in Fig. 6d and e. These results regarding 1D Sb_2Se_3 nanostructures indicate the importance of controlling both the morphology and crystallographic orientation of anisotropic Sb_2Se_3 to achieve enhanced PEC performance.

2.3 Co-catalysts for Sb_2Se_3 photocathodes

Because light absorbers and protective layers generally have poor catalytic activity, most efficient photocathodes include co-catalysts with low overpotential for HERs. The deposition conditions of co-catalysts must be carefully controlled to achieve high performance because metallic catalysts, such as Pt, can reflect incident light, thereby reducing overall performance. Co-catalyst materials, as well as the deposition methods, are surveyed in a comprehensive review paper by Roger *et al.*[52] One of the widely used methods for co-catalyst deposition is the photodeposition of Pt.[21] In addition, it was also reported that the formation of a heterojunction with ammonium thiomolybdate plays a similar role in boosting the catalytic activity.[20,53] Thus far, three HER co-catalysts have been used in Sb_2Se_3 photocathodes: Pt, RuO_x, and MoS_x. For the deposition of Pt co-catalysts on Sb_2Se_3 photocathodes, both photo-electrodeposition (PED)[41,50] and sputtering[32,51,54,55] methods have been used. In general, sputtering is unsuitable for the conformal coating of complicated nanostructures because the
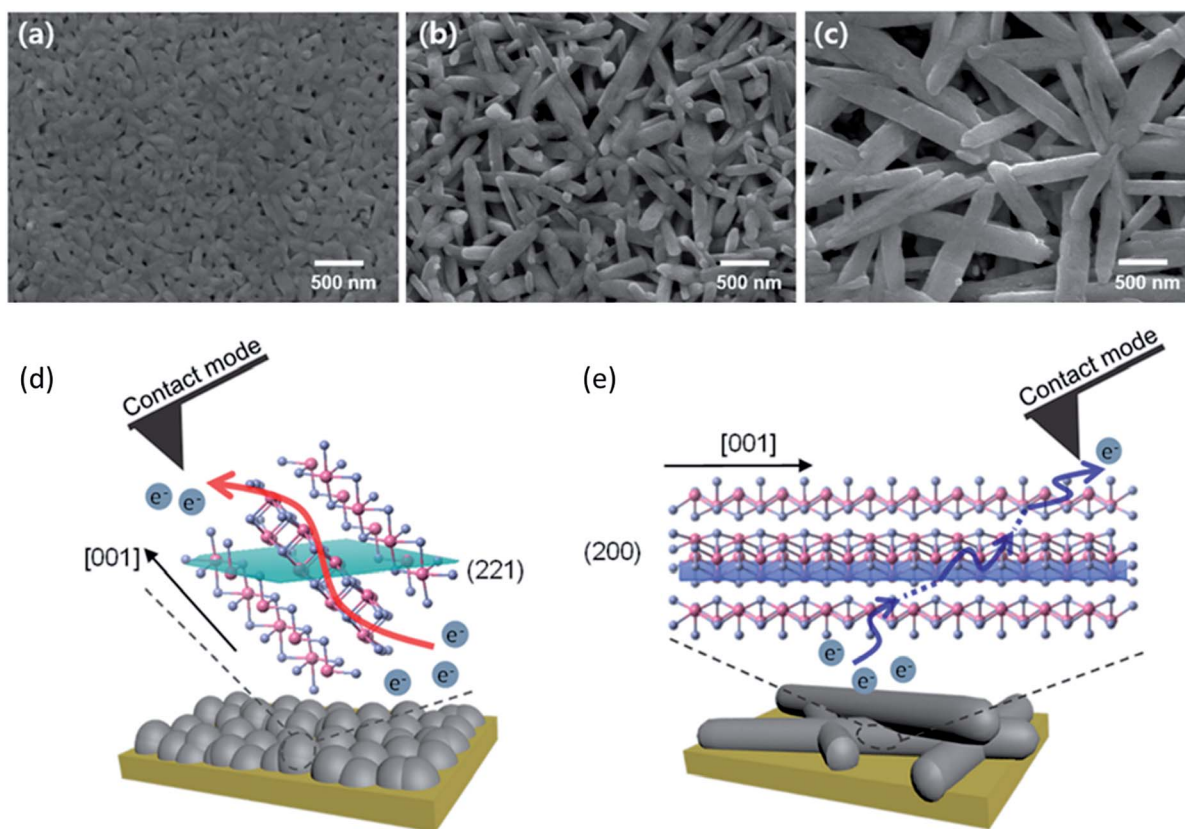
Fig. 6 (a–c) Morphological evolution of Sb_2Se_3 thin films with the Sb-to-Se ratio of (a) 1.5, (b) 4, (c) 6 in a solvent ink. Schematic images illustrating different charge-transport pathways in (d) planar Sb_2Se_3 thin films and (e) Sb_2Se_3 nanowire films. Reprinted with permission from ref. 51. Copyright (2019) American Chemical Society.

This journal is © The Royal Society of Chemistry 2019

J. Mater. Chem. A, 2019, 7, 20467–20477 | 20471

sputtering source is unable to reach the bottom of a nano-structured semiconductor. The PED method can be applied to complicated structures, but it is difficult to obtain well-dispersed uniform Pt nanoparticles using the PED method because growth sites are randomly distributed.[56] Therefore, a more delicate method for the decoration of Pt, such as a two-step platinization strategy,[56] should be considered for maximizing the performance of Sb_2Se_3 photocathodes. However, there is little information available regarding the effects of Pt deposition conditions on the performance of Sb_2Se_3 photocathodes based on their relatively short development history. Only one study has mentioned that Pt deposition stability is dependent on PED time, where it was determined that much better stability of $Pt/TiO_2/Sb_2Se_3/Au/FTO$ photocathodes can be observed with increasing Pt deposition time.[50]

One important issue regarding co-catalysts for PEC water splitting is the exploration of alternative earth-abundant catalytic materials and development of proper deposition techniques.[52] MoS_x is an attractive HER catalyst because of its abundance and high HER activity in acidic electrolytes. Two different types of Sb_2Se_3 photocathode configurations were reported using MoS_x catalysts: $MoS_x/Sb_2Se_3/Au/FTO$[44] and $MoS_x/TiO_2/Sb_2Se_3/Au/FTO$.[57] In the first configuration, without a TiO_2 layer, MoS_x was directly deposited onto Sb_2Se_3 via PED, followed by post-sulfurization at 250 °C. The authors insisted that post-sulfurization converts the Sb_2O_3 on the surface of Sb_2Se_3 into Sb_2S_3, forming an effective hole-blocking contact and leading to earlier photocurrent onset. Tan et al. reported a more in-depth deposition mechanism of MoS_x on TiO_2/Sb_2Se_3 junctions by elucidating CV scans.[57] As shown in Fig. 7a and b, the morphology of MoS_x on TiO_2/Sb_2Se_3 is strongly dependent on the starting potential applied during the first cycle of voltage sweeping. Cathodically initiated MoS_x (denoted as CI-MoS_x, i.e., prepared with a potential starting at -0.3 V_{RHE}) exhibits a film-like uniform structure, whereas non-uniform island structures can be observed for anodically initiated MoS_x (denoted as AI-MoS_x, i.e., prepared with a potential starting at 0.6 V_{RHE}). As a result, CI-MoS_x-based Sb_2Se_3 photocathodes exhibit four

times the photocurrent density of their AI-MoS_x-based counterparts as shown in Fig. 7c and d. Such efforts focused on implementing earth-abundant co-catalysts for Sb_2Se_3 photocathodes will pave the way toward low-cost photoelectrode production.

2.4 Top interface engineering for Sb_2Se_3 photocathodes

The first Sb_2Se_3 photocathode for solar hydrogen generation was prepared by depositing a TiO_2 layer on top of $Sb_2Se_3/Au/FTO$ using atomic layer deposition (ALD), followed by Pt co-catalyst deposition (i.e., $Pt/TiO_2/Sb_2Se_3/Au/FTO$). Since then, various configurations for Sb_2Se_3 photocathodes have been implemented, including $MoS_x/Sb_2Se_3/Au/FTO$,[44] $MoS_x/TiO_2/Sb_2Se_3/Au/FTO$,[57] $RuO_x/TiO_2/Sb_2Se_3/Au/FTO$,[36] $Pt/C_{60}/TiO_2/Sb_2Se_3/Au/FTO$,[54] $Pt/TiO_2/CdS/Sb_2Se_3/Au/FTO$,[51] and $Pt/TiO_2/CdS/Sb_2Se_3/Mo/FTO$.[41] In this subsection, we focus on the top interface above Sb_2Se_3, and below any co-catalysts. The bottom interface will be discussed in the following sections.

Thin TiO_2 layers have been widely used in various photocathodes for PEC water splitting, as a protective layer and n-type junction layer, based on the dual-role of their n-type semiconducting properties and photocorrosion stability in electrolytes.[58-62] Furthermore, ALD is a suitable technique for depositing high-quality thin films on top of delicate nanostructures. Using ALD, a conformal TiO_2 layer was successfully deposited on Sb_2Se_3 nanoneedle arrays (Fig. 8a-e) and the resulting device exhibited a noteworthy photocurrent level (approximately in mA scale) and hydrogen generation via water splitting.[32] Although TiO_2–Sb_2Se_3 systems have well-aligned conduction band minimums (CBMs) for favorable water reduction potential, the E_g value of TiO_2 (approximately 3.2 eV) is much greater than that of Sb_2Se_3 (approximately 1.2 eV), resulting in large mismatches between valence band maximums. It was found that n-type CdS (E_g value of approximately 2.4 eV) can act as a buffer layer for enhancing the onset potential of Sb_2Se_3 photocathodes.[51] As shown in Fig. 8f, the onset potential of a planar Sb_2Se_3 thin film photocathode
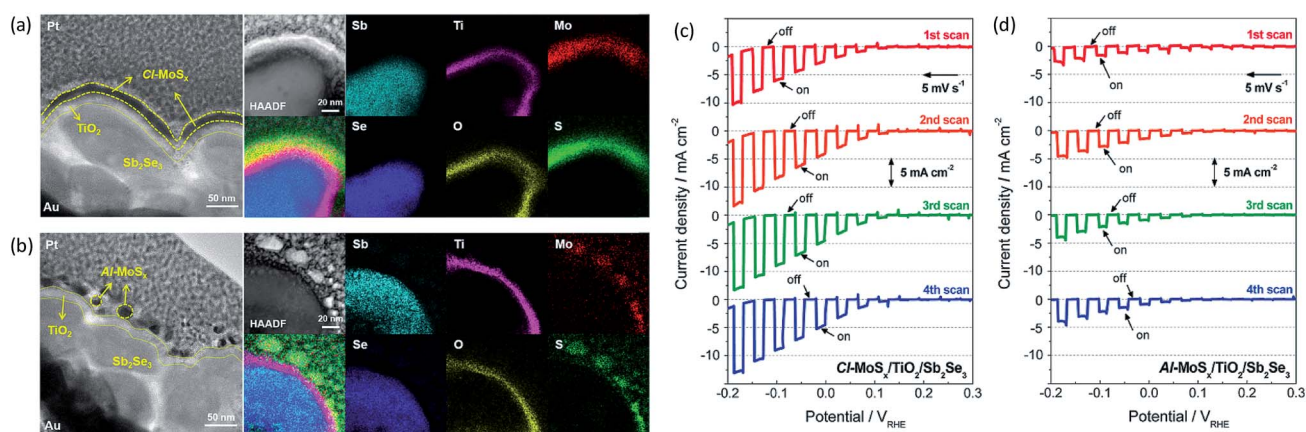
Fig. 7 TEM images and EDS mapping results showing the microstructures of (a) CI-$MoS_x/TiO_2/Sb_2Se_3$ and (b) AI-$MoS_x/TiO_2/Sb_2Se_3$ photocathodes. Current density–potential curves of (c) CI-$MoS_x/TiO_2/Sb_2Se_3$ and (d) AI-$MoS_x/TiO_2/Sb_2Se_3$ photocathodes. Reprinted with permission from ref. 57. Copyright (2018) American Chemical Society.

20472 | J. Mater. Chem. A, 2019, **7**, 20467–20477

This journal is © The Royal Society of Chemistry 2019
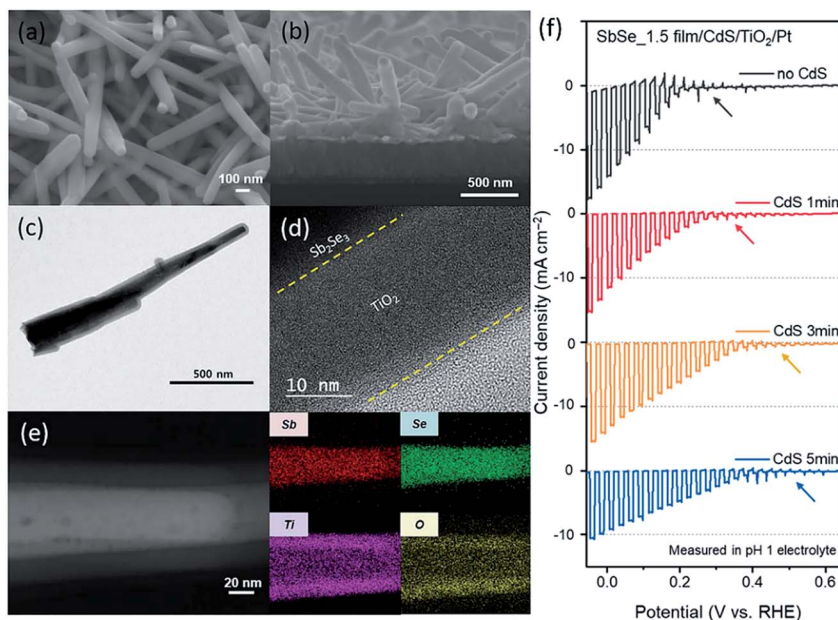
Fig. 8 (a) Top-view and (b) side-view scanning electron microscopy images of Sb_2Se_3 nanoneedles modified with TiO_2. (c) Low-resolution transmission electron microscopy (TEM) image and (d) high-resolution TEM image of TiO_2/Sb_2Se_3. (e) High-angle annular dark-field scanning TEM image and corresponding energy-dispersive X-ray spectroscopy (EDS) elemental mapping of TiO_2/Sb_2Se_3. Reproduced from ref. 32 with permission from The Royal Society of Chemistry. (f) Current density–potential curves of planar Sb_2Se_3 thin-film-based photocathodes with different CdS deposition times. Reprinted with permission from ref. 51. Copyright (2019) American Chemical Society.

increases following the addition of a CdS layer between the Sb_2Se_3 and TiO_2. It has been hypothesized that this increased onset potential is a result of enhanced hole extraction through the CdS layer. However, the photocurrent decreases with an increasing thickness of the CdS layer, based on small spikes in

the CBMs between Sb_2Se_3 and CdS. It is noteworthy that in buried junction photoelectrodes for PEC water splitting, photovoltage is determined by the heterojunctions of semiconductor materials.[63] Thus far, the maximum onset potential (0.47 V_{RHE}) obtained by an Sb_2Se_3 photocathode was achieved
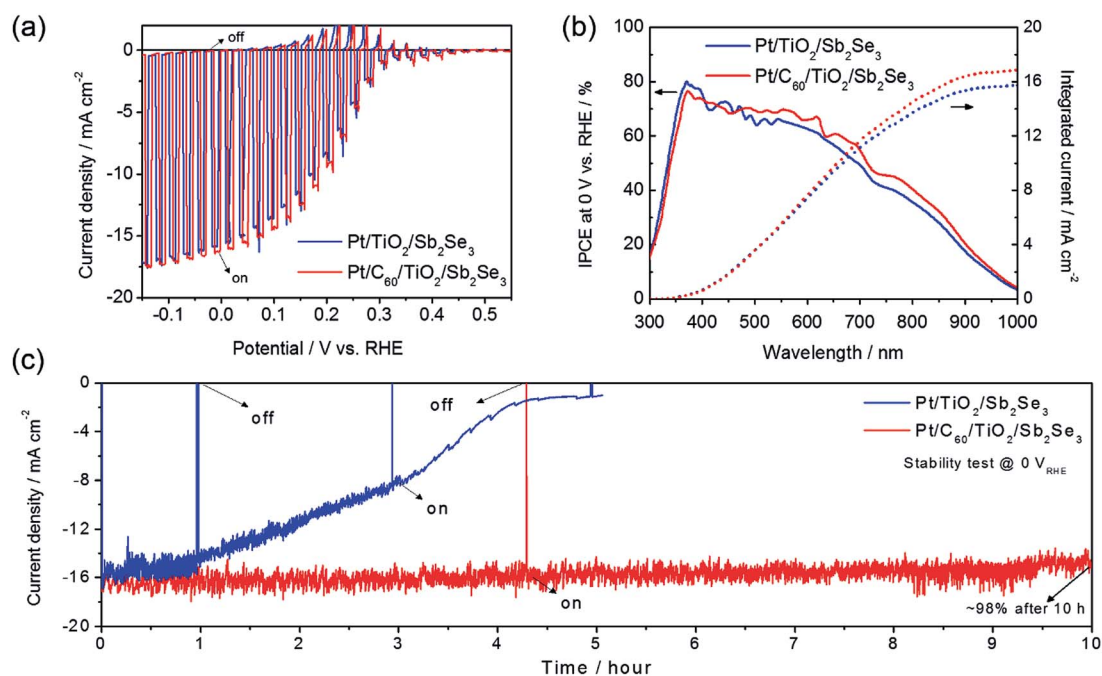
Fig. 9 (a) Current density–potential curves, (b) incident photon-to-current conversion efficiency, and (c) stability tests of Sb_2Se_3 photocathodes with and without C_{60} layers. Reproduced from ref. 54 with permission from John Wiley & Sons, Inc.
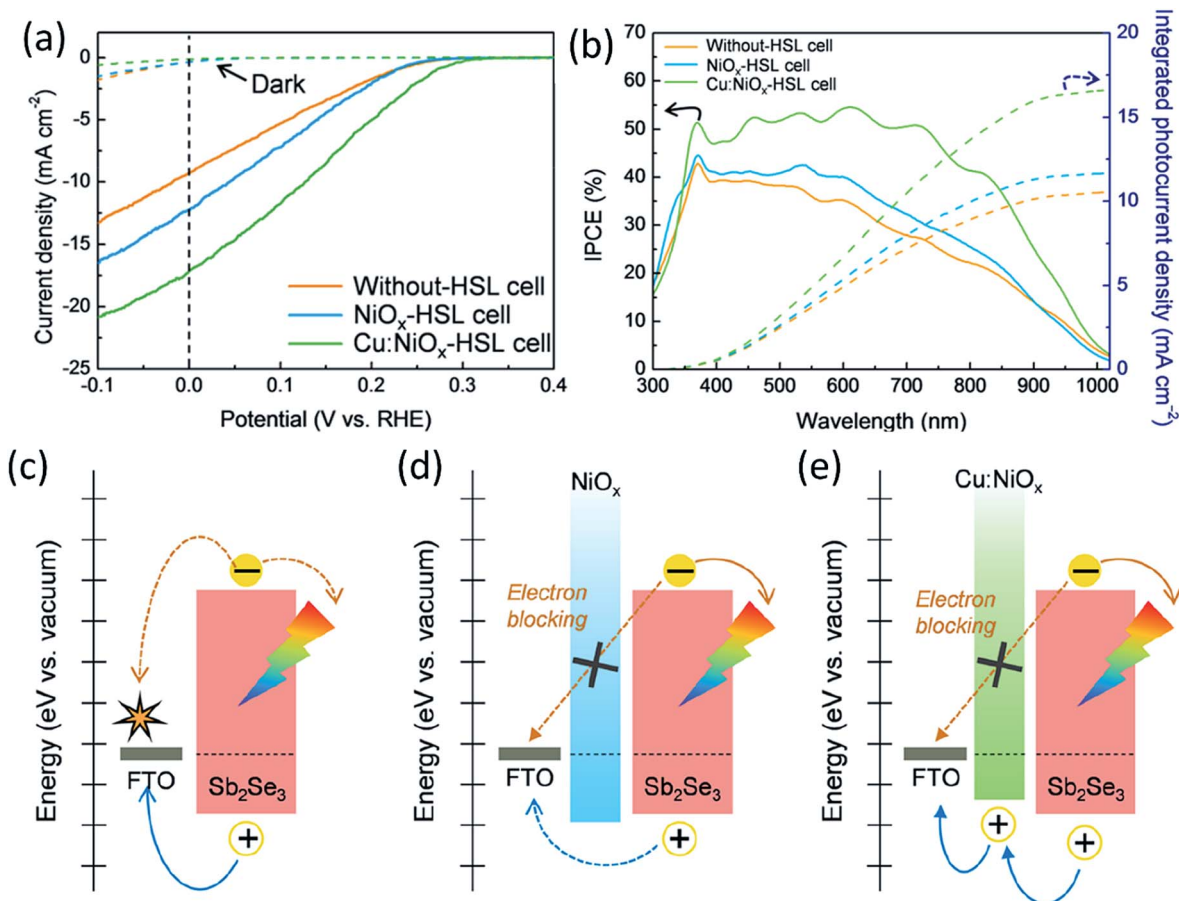
Fig. 10 (a) Current density–potential and (b) incident photon-to-current conversion efficiency curves of Sb_2Se_3 photocathodes with three different HSLs. Band energy diagram after equilibrium for (c) without-HSL cell, (d) NiO_x-HSL cell, and (e) $Cu:NiO_x$-HSL cell. The work function of FTO is located at near 4.5 eV (with respect to the vacuum level), which is vicinity to the HER. Reprinted with permission from ref. 55. Copyright (2019) American Chemical Society.

with a $TiO_2/CdS/Sb_2Se_3$ junction in which Sb_2Se_3 thin films were prepared by either solution processing[51] or thermal evaporation.[41] However, CdS is a notoriously toxic material and Cd diffusion along the gaps between $(Sb_4Se_6)_n$ ribbons can lead to severe stability issues.[64] Therefore, it is necessary to develop alternative non-toxic buffer layers and/or n-type junction layers that are suitable for achieving high photovoltage and stability.

In addition to the n-type semiconductors of CdS and TiO_2, fullerene (C_{60}) has been used in Sb_2Se_3 photocathodes as a top interface engineering material.[54] C_{60} was deposited between TiO_2 and a Pt catalyst in a configuration of $Pt/C_{60}/TiO_2/Sb_2Se_3/Au/FTO$. With the addition of a C_{60} layer, the stability of the Sb_2Se_3 photocathodes was significantly enhanced. No noticeable degradation was observed up to 10 h and there was no significant change in initial performance, as shown in Fig. 9. Without a C_{60} layer, the transfer rate of photo-excited electrons from the TiO_2 layer to the Pt catalyst is sluggish, meaning that these electrons contribute to the photo-reduction of TiO_2 instead of hydrogen evolution reactions (HERs). In contrast, with a C_{60} layer, the charge transfer rate is significantly improved and the photo-reduction of TiO_2 is prevented, eventually leading to the enhanced stability of Sb_2Se_3 photocathodes.

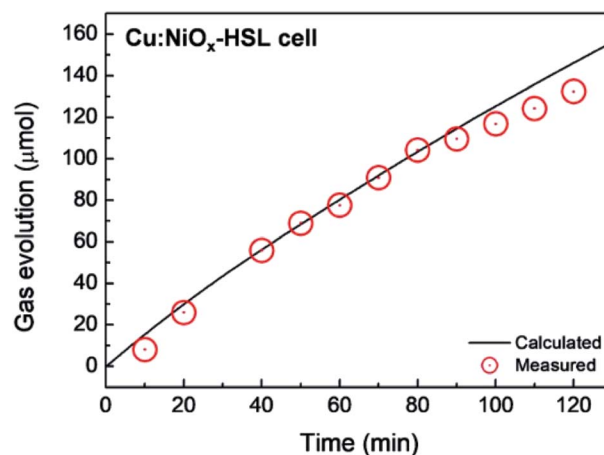Fig. 11 Time-course curve of H_2 evolution for the $Cu:NiO_x$-HSL cell. The solid line represents the calculated H_2 evolution, and the circular dots represent the H_2 evolution measured via gas chromatography. Reprinted with permission from ref. 55. Copyright (2019) American Chemical Society.

20474 | J. Mater. Chem. A, 2019, 7, 20467–20477

This journal is © The Royal Society of Chemistry 2019

Table 1 Summary of Sb_2Se_3 for PEC water splitting[a]

Year	Preparation methods	Device structure	Photocurrent (mA cm^{-2} @ 0 V$_{RHE}$)	Stability (J/J_o)*; time	Note	Ref.
2017	Solution processing (TGA + EA)	FTO/Au/Sb_2Se_3/TiO$_2$/Pt	~2.5	10%; 3 h	The first Sb_2Se_3 photocathode	32
2017	Electrodeposition of Sb + selenization	FTO/Au/Sb_2Se_3/MoS$_x$	~16	~90%; 20 h	Photocorrosion resistant Sb_2Se_3	44
2017	Thermal evaporation	FTO/Mo/Sb_2Se_3/CdS/TiO$_2$/Pt	8.6	~85%; 10 h	Large area > 20 cm^2	41
2018	Solution processing (TGA + EA)	FTO/Au/Sb_2Se_3/TiO$_2$/Pt	12.5	~55%; 2 h		50
2018	Solution processing (TGA + EA)	FTO/Au/Sb_2Se_3/TiO$_2$/MoS$_x$	4.8	~12%; 15 m		57
2019	Solution processing (TGA + EA)	FTO/Au/Sb_2Se_3/TiO$_2$/C$_{60}$/Pt	17	~98%; 10 h		54
2019	Solution processing (TGA + EA)	FTO/Cu:NiO/Sb_2Se_3/TiO$_2$/Pt	17.5	~75%; 4 h		55
2019	Solution processing (2-mercaptoethanol + ethylenediamine)	FTO/Au/Sb_2Se_3/CdS/TiO$_2$/Pt	11	~73%; 3 h		51

[a] (J/J_o)* presents the ratio of the measured photocurrent after the stability test time @ 0 V$_{RHE}$ with respect to the initial photocurrent.

2.5 Bottom interface engineering for Sb_2Se_3 photocathodes

In a typical photocathode, photo-excited electrons should move toward the surface of the semiconductor to drive HERs and photo-excited holes should be extracted through the bottom contact and reach the counter electrode for oxygen evolution reactions. From this perspective, a proper hole selective layer (HSL) should be developed to facilitate hole extraction through bottom contacts. Both Sb_2Se_3 photocathodes for PEC water splitting and Sb_2Se_3 solar cells typically employ Au as a back contact layer based on its proper band alignment with Sb_2Se_3 band positions, as well as its good stability and electrical properties. In Sb_2Se_3 solar cell research, a thorough investigation of alternative back contacts was performed by Zhang et al.[65] They concluded that a NiO$_x$/Ni layer can serve as an attractive low-cost alternative to an Au back contact and suggested leveraging the improved electrical properties of a NiO$_x$ layer to reduce series resistance. A similar strategy was reported in a PEC water splitting study, where a Cu doping strategy was adopted to improve the conductivity of a NiO$_x$ layer, leading to the enhanced photocurrent density of Sb_2Se_3 photocathodes.[55] As shown in Fig. 10a and b, the performance of Sb_2Se_3 photocathodes improves slightly when a NiO$_x$ layer is used as an HSL, but much better performance can be observed with a Cu:NiO$_x$ HSL. It can be concluded that photo-excited electrons and holes recombine at the back contact in the absence of an HSL, as shown in Fig. 10c. As proven by electrochemical impedance spectroscopy and ultraviolet photoelectron spectroscopy results, a NiO layer is able to prevent back recombination by blocking electron backflow, but hole extraction is sluggish based on high resistance (Fig. 10d). In contrast, a Cu:NiO layer is advantageous for both preventing recombination and promoting hole extraction based on its improved conductivity. Gas chromatography was used to confirm that the photocurrent obtained by the Cu:NiO$_x$-HSL cell corresponded to the HER without any side reactions, revealing nearly 100% faradaic efficiency (Fig. 11). It is noteworthy that Cu:NiO was reported at almost the same time in a different study on an earth-abundant CuBi$_2$O$_4$ photocathode as an effective HSL,[66] indicating that research interest in earth-abundant HSL materials for improving the performance of photocathodes is increasing.

3. Conclusion and outlooks

It is widely accepted that the success of commercial solar hydrogen production depends on the successful discovery of cost-effective semiconductors that are suitable for high-performance PEC devices. The meteoric rise of Sb_2Se_3 suggests a bright future in the area of STH conversion due to its unique characteristics that distinguish it from other semiconductor materials. Among the promising features of Sb_2Se_3, its stability against photocorrosion and excellent processability are prominent advantages for practical STH conversion. A summary of Sb_2Se_3 photocathodes for PEC water splitting research is shown in Table 1. Although Sb_2Se_3 has received significant attention during its short history, there remains ample scope for further investigation and improvement. Previously reported solution-based approaches to utilizing Sb_2Se_3 depend on relatively toxic solvents, such as TGA and 2-mercaptoethanol, meaning non-toxic and environmentally friendly solution-based synthetic routes must be developed. Another important issue for Sb_2Se_3 is its relatively low onset potential, with a maximum reported value among previous studies of approximately 0.47 V$_{RHE}$.[51] Proper buried junction formation (similar to the case of Cu$_2$O, where onset potential is significantly enhanced by a Ga$_2$O$_3$ junction layer)[67] and the interfacial dipole strategy[68] can provide promising solutions to increasing the onset potential of Sb_2Se_3 photocathodes. As discussed in Section 2.4, a non-toxic junction layer free from inter-diffusion issues, for enhancing photovoltage, should also be explored. However, according to a recent theoretical study by Huang et al.,[69] the predicted maximum achievable photovoltage of an Sb_2Se_3 photoelectrode is approximately 0.47 V based on its indirect E_g value and complicated defect states caused by its quasi-1D structure. They suggested that strain engineering to reduce the space between quasi 1D ribbons or sandwich inter-ribbon spaces with bulky and inert spacers could be helpful for increasing the formation energy of

This journal is © The Royal Society of Chemistry 2019

J. Mater. Chem. A, 2019, 7, 20467–20477 | 20475

deep defects and enhancing photovoltage. However, it is known that doping Sb_2Se_3 generally leads to harmful effects because dopants are often inserted into the inter-ribbon space instead of replacing Sb and Se lattice sites.[10,70] Therefore, further in-depth theoretical calculations in combination with experimental verification should be performed to find an effective method for the defect engineering of Sb_2Se_3. Additionally, unassisted water splitting by fabricating a tandem device connected to a different type of light absorber should be investigated to determine the feasibility of practical solar hydrogen production using an Sb_2Se_3 light absorber. For example, we can envision a tandem device consisting of an Sb_2Se_3 photocathode and a $BiVO_4$ photoanode, which has been the most successful photoanode material for PEC tandem devices.[4] Because the onset potential and photocurrent density at 0.4 V_{RHE} of state-of-the-art $BiVO_4$ photoanodes are approximately 0.2 V_{RHE} and 1.5 mA cm^{-2},[71] respectively, the onset potential of the Sb_2Se_3 photocathode must be at least 0.5 V_{RHE} with an acceptable fill factor to achieve meaningful STH efficiency. Additionally, the electrolyte compatibility of Sb_2Se_3 photocathodes should be verified because most $BiVO_4$ photoanodes generally achieve high performance in neutral or weak basic electrolytes. Because most previously reported Sb_2Se_3 photocathodes were tested in dilute H_2SO_4 (pH of 0–1) or a phosphate-buffered electrolyte (pH of approximately 6.5), the performance and stability of Sb_2Se_3 in different electrolytes, such as potassium biphosphate and potassium borate, which are known to be compatible with efficient $BiVO_4$ photoanodes, should be investigated. Additionally, utilizing a bipolar membrane could be an attractive solution for possible electrolyte incompatibility issues and fabricating efficient PEC tandem devices with Sb_2Se_3 photocathodes. Ultimately, a real large-area device using an Sb_2Se_3 photocathode should be fabricated in the future to overcome the "artificial photosynthetic leaf-to-farm challenge".[4] We hope to see the participation of scientists and engineers from around the world to advance Sb_2Se_3 photocathodes for solar hydrogen production.

Conflicts of interest

There are no conflicts to declare.

Acknowledgements

References

1 A. Fujishima and K. Honda, *Nature*, 1972, **238**, 37–38.
2 S. Ardo, D. F. Rivas, M. A. Modestino, V. S. Greiving, F. F. Abdi, E. A. Llado, V. Artero, K. Ayers, C. Battaglia and J.-P. Becker, *Energy Environ. Sci.*, 2018, **11**, 2768–2783.
3 H. Thomas, F. Armstrong, N. Brandon, B. David, A. Barron, J. Durrant, A. Guwy, A. Kucernak, M. Lewis, J. Maddy, I. Metcalfe and A. Porch, *Options for producing low-carbon hydrogen at scale*, The Royal Society, 2018.
4 J. H. Kim, D. Hansora, P. Sharma, J.-W. Jang and J. S. Lee, *Chem. Soc. Rev.*, 2019, **48**, 1908–1971.
5 W.-H. Cheng, M. H. Richter, M. M. May, J. Ohlmann, D. Lackner, F. Dimroth, T. Hannappel, H. A. Atwater and H.-J. Lewerenz, *ACS Energy Lett.*, 2018, **3**, 1795–1800.
6 M. A. Green, *Nat. Energy*, 2016, **1**, 15015.
7 M. R. Shaner, H. A. Atwater, N. S. Lewis and E. W. McFarland, *Energy Environ. Sci.*, 2016, **9**, 2354–2371.
8 J. A. Turner, *Science*, 2014, **344**, 469–470.
9 K. Sivula and R. Van De Krol, *Nat. Rev. Mater.*, 2016, **1**, 15010.
10 W. Yang and J. Moon, *ChemSusChem*, 2018, **12**, 1889–1899.
11 P. Sharma, J. W. Jang and J. S. Lee, *ChemCatChem*, 2019, **11**, 157–179.
12 J. Luo, L. Steier, M.-K. Son, M. Schreier, M. T. Mayer and M. Grätzel, *Nano Lett.*, 2016, **16**, 1848–1857.
13 A. Paracchino, J. C. Brauer, J.-E. Moser, E. Thimsen and M. Graetzel, *J. Phys. Chem. C*, 2012, **116**, 7341–7350.
14 A. Paracchino, V. Laporte, K. Sivula, M. Grätzel and E. Thimsen, *Nat. Mater.*, 2011, **10**, 456.
15 M. S. Prévot, N. Guijarro and K. Sivula, *ChemSusChem*, 2015, **8**, 1359–1367.
16 M. S. Prévot, X. A. Jeanbourquin, W. S. Bourée, F. Abdi, D. Friedrich, R. Van De Krol, N. s. Guijarro, F. Le Formal and K. Sivula, *Chem. Mater.*, 2017, **29**, 4952–4962.
17 C.-M. Jiang, S. E. Reyes-Lillo, Y. Liang, Y.-S. Liu, G. Liu, F. M. Toma, D. Prendergast, I. D. Sharp and J. K. Cooper, *Chem. Mater.*, 2019, **31**, 2524–2534.
18 A. Hankin, F. Bedoya-Lora, C. Ong, J. Alexander, F. Petter and G. Kelsall, *Energy Environ. Sci.*, 2017, **10**, 346–360.
19 J. R. Mckone, A. P. Pieterick, H. B. Gray and N. S. Lewis, *J. Am. Chem. Soc.*, 2013, **135**, 223–231.
20 F. Bozheyev, F. Xi, P. Plate, D. Thomas, S. Fiechter and K. Ellmer, *J. Mater. Chem. A*, 2019, **7**, 10769–10780.
21 F. Bozheyev, K. Harbauer, C. Zahn, D. Friedrich and K. Ellmer, *Sci. Rep.*, 2017, **7**, 16003.
22 F. Bozheyev, M. Rengachari, S. P. Berglund, D. A. Ras and K. Ellmer, *Mater. Sci. Semicond. Process.*, 2019, **93**, 284–289.
23 X. Yu, M. S. Prevot, N. Guijarro and K. Sivula, *Nat. Commun.*, 2015, **6**, 7596.
24 X. Yu, N. Guijarro, M. Johnson and K. Sivula, *Nano Lett.*, 2018, **18**, 215–222.
25 N. Tideswell, F. Kruse and J. McCullough, *Acta Crystallogr.*, 1957, **10**, 99–102.
26 M. Coutts and E. Levin, *J. Appl. Phys.*, 1967, **38**, 4039–4044.
27 S. Shutov, V. Sobolev, Y. V. Popov and S. Shestatskii, *Phys. Status Solidi B*, 1969, **31**, K23–K27.
28 N. Platakis, V. Sadagopan and H. Gatos, *J. Electrochem. Soc.*, 1969, **116**, 1436–1439.
29 Y. Zhou, M. Leng, Z. Xia, J. Zhong, H. Song, X. Liu, B. Yang, J. Zhang, J. Chen, K. Zhou, J. Han, Y. Cheng and J. Tang, *Adv. Energy Mater.*, 2014, **4**, 1301846.
30 Y. C. Choi, T. N. Mandal, W. S. Yang, Y. H. Lee, S. H. Im, J. H. Noh and S. I. Seok, *Angew. Chem., Int. Ed.*, 2014, **53**, 1329–1333.

31 Z. Li, X. Liang, G. Li, H. Liu, H. Zhang, J. Guo, J. Chen, K. Shen, X. San and W. Yu, *Nat. Commun.*, 2019, **10**, 125.

32 J. Kim, W. Yang, Y. Oh, H. Lee, S. Lee, H. Shin, J. Kim and J. Moon, *J. Mater. Chem. A*, 2017, **5**, 2180–2187.

33 R. K. Zinke, W. H. Werkheiser and J. A. Ober, *U.S. Department of the interior, U.S. Geological Survey*, 2018, DOI: 10.3133/70194932.

34 Abundance in Earth's Crust of the elements, DOI: http://periodictable.com/Properties/A/CrustAbundance.html.

35 C. Chen, D. C. Bobela, Y. Yang, S. Lu, K. Zeng, C. Ge, B. Yang, L. Gao, Y. Zhao, M. C. Beard and J. Tang, *Front. Optoelectron.*, 2017, **10**, 18–30.

36 W. Yang, S. Lee, H.-C. Kwon, J. Tan, H. Lee, J. Park, Y. Oh, H. Choi and J. Moon, *ACS Nano*, 2018, **12**, 11088–11097.

37 Y. Zhou, L. Wang, S. Chen, S. Qin, X. Liu, J. Chen, D.-J. Xue, M. Luo, Y. Cao and Y. Cheng, *Nat. Photonics*, 2015, **9**, 409.

38 O. S. Hutter, L. J. Phillips, K. Durose and J. D. Major, *Sol. Energy Mater. Sol. Cells*, 2018, **188**, 177–181.

39 X. Wen, C. Chen, S. Lu, K. Li, R. Kondrotas, Y. Zhao, W. Chen, L. Gao, C. Wang and J. Zhang, *Nat. Commun.*, 2018, **9**, 2179.

40 K. Li and J. Tang, *J. Photonics Energy*, 2018, PT4B.19.

41 L. Zhang, Y. Li, C. Li, Q. Chen, Z. Zhen, X. Jiang, M. Zhong, F. Zhang and H. Zhu, *ACS Nano*, 2017, **11**, 12753–12763.

42 G. Ghosh, *J. Phase Equilib.*, 1993, **14**, 753–763.

43 I. Efthimiopoulos, J. Zhang, M. Kucway, C. Park, R. C. Ewing and Y. Wang, *Sci. Rep.*, 2013, **3**, 2665.

44 R. R. Prabhakar, W. Septina, S. Siol, T. Moehl, R. Wick-Joliat and S. D. Tilley, *J. Mater. Chem. A*, 2017, **5**, 23139–23145.

45 S. Hu, C. Xiang, S. Haussener, A. D. Berger and N. S. Lewis, *Energy Environ. Sci.*, 2013, **6**, 2984–2993.

46 M. S. Prévot and K. Sivula, *J. Phys. Chem. C*, 2013, **117**, 17879–17893.

47 H. Kobayashi, N. Sato, M. Orita, Y. Kuang, H. Kaneko, T. Minegishi, T. Yamada and K. Domen, *Energy Environ. Sci.*, 2018, **11**, 3003–3009.

48 M. Birkett, W. M. Linhart, J. Stoner, L. J. Phillips, K. Durose, J. Alaria, J. D. Major, R. Kudrawiec and T. D. Veal, *APL Mater.*, 2018, **6**, 084901.

49 R. Vadapoo, S. Krishnan, H. Yilmaz and C. Marin, *Phys. Status Solidi B*, 2011, **248**, 700–705.

50 W. Yang, J. Ahn, Y. Oh, J. Tan, H. Lee, J. Park, H. C. Kwon, J. Kim, W. Jo and J. Kim, *Adv. Energy Mater.*, 2018, **8**, 1702888.

51 J. Park, W. Yang, Y. Oh, J. Tan, H. Lee, R. Boppella and J. Moon, *ACS Energy Lett.*, 2019, **4**, 517–526.

52 I. Roger, M. A. Shipman and M. D. Symes, *Nat. Rev. Chem.*, 2017, **1**, 0003.

53 F. Xi, P. Bogdanoff, K. Harbauer, P. Plate, C. Hohn, J. Rappich, B. Wang, W. Han, R. van de Krol and S. Fiechter, *ACS Catal.*, 2019, **9**, 2368–2380.

54 J. Tan, W. Yang, Y. Oh, H. Lee, J. Park, R. Boppella, J. Kim and J. Moon, *Adv. Energy Mater.*, 2019, **9**, 1900179.

55 H. Lee, W. Yang, J. Tan, Y. Oh, J. Park and J. Moon, *ACS Energy Lett.*, 2019, **4**, 995–1003.

56 M. Chen, Y. Liu, C. Li, A. Li, X. Chang, W. Liu, Y. Sun, T. Wang and J. Gong, *Energy Environ. Sci.*, 2018, **11**, 2025–2034.

57 J. Tan, W. Yang, Y. Oh, H. Lee, J. Park and J. Moon, *ACS Appl. Mater. Interfaces*, 2018, **10**, 10898–10908.

58 D. Bae, B. Seger, P. C. Vesborg, O. Hansen and I. Chorkendorff, *Chem. Soc. Rev.*, 2017, **46**, 1933–1954.

59 W. Yang, Y. Oh, J. Kim, M. J. Jeong, J. H. Park and J. Moon, *ACS Energy Lett.*, 2016, **1**, 1127–1136.

60 Y.-X. Yu, L. Pan, M.-K. Son, M. T. Mayer, W.-D. Zhang, A. Hagfeldt, J. Luo and M. Grätzel, *ACS Energy Lett.*, 2018, **3**, 760–766.

61 Y. Zhou, D. Shin, E. Ngaboyamahina, Q. Han, C. B. Parker, D. B. Mitzi and J. T. Glass, *ACS Energy Lett.*, 2017, **3**, 177–183.

62 K. Wang, D. Huang, L. Yu, K. Feng, L. Li, T. Harada, S. Ikeda and F. Jiang, *ACS Catal.*, 2019, **9**, 3090–3097.

63 M. T. Mayer, *Curr. Opin. Electrochem.*, 2017, **2**, 104–110.

64 L. Wang, D.-B. Li, K. Li, C. Chen, H.-X. Deng, L. Gao, Y. Zhao, F. Jiang, L. Li, F. Huang, Y. He, H. Song, G. Niu and J. Tang, *Nat. Energy*, 2017, **2**, 17046.

65 J. Zhang, R. Kondrotas, S. Lu, C. Wang, C. Chen and J. Tang, *Sol. Energy*, 2019, **182**, 96–101.

66 A. Song, P. Plate, A. Chemseddine, F. Wang, F. Abdi, M. Wollgarten, R. van de Krol and S. Berglund, *J. Mater. Chem. A*, 2019, **7**, 9183–9194.

67 C. Li, T. Hisatomi, O. Watanabe, M. Nakabayashi, N. Shibata, K. Domen and J.-J. Delaunay, *Energy Environ. Sci.*, 2015, **8**, 1493–1500.

68 R. Wick-Joliat, T. Musso, R. R. Prabhakar, J. Löckinger, S. Siol, W. Cui, L. Sévery, T. Moehl, J. Suh and J. Hutter, *Energy Environ. Sci.*, 2019, **12**, 1901–1909.

69 M. Huang, P. Xu, D. Han, J. Tang and S. Chen, *ACS Appl. Mater. Interfaces*, 2019, **11**, 15564–15572.

70 Y. Li, Y. Zhou, Y. Zhu, C. Chen, J. Luo, J. Ma, B. Yang, X. Wang, Z. Xia and J. Tang, *Appl. Phys. Lett.*, 2016, **109**, 232104.

71 J. H. Kim and J. S. Lee, *Adv. Mater.*, 2019, **31**, 1806938.

This journal is © The Royal Society of Chemistry 2019

J. Mater. Chem. A, 2019, **7**, 20467–20477 | **20477**